Journal of Organometallic Chemistry 897 (2019) 192–199

Contents lists available at ScienceDirect

Journal of Organometallic Chemistry

journal homepage: www.elsevier.com/locate/jorganchem

Synthesis and characterization of platinum(II) polymetallaynes functionalized with phenoxazine-based spacer. A comparison with the phenothiazine congener

Wai-Yeung Wong [a, b, c, **], Li Li [b], Lei Wang [a, *]

[a] Shenzhen Key Laboratory of Polymer Science and Technology, College of Materials and Engineering, Shenzhen University, Shenzhen, 518060, China
[b] Department of Chemistry, Hong Kong Baptist University, Kowloon Tong, Hong Kong, China
[c] Department of Applied Biology and Chemical Technology, The Hong Kong Polytechnic University, Hung Hom, Hong Kong, China

ARTICLE INFO

Article history:
Received 31 May 2019
Received in revised form
24 June 2019
Accepted 27 June 2019
Available online 27 June 2019

Keywords:
Phenoxazine
Metallopolyyne
Platinum
Solar cell
Thiophene

ABSTRACT

A new series of soluble, solution-processable metallopolyynes of platinum(II) functionalized with electron-rich phenoxazine–oligothiophene rings and their corresponding dinuclear model complexes were synthesized and characterized. The influence of the inclusion of thienyl rings along the polymer chain on the optical, electronic and photovoltaic properties of these metallopolymers was studied. The evolution of the singlet and triplet excited states in these metal-based materials was elucidated in detail. It is shown that addition of the thiophene rings can elevate the HOMO energy level of the polymers. The absorption edge of the oxygen analogue is more red-shifted than that of the sulfur congener, which is attributed to the stronger electron-donating ability of the phenoxazine unit than that of the phenothiazine group. The down-shifted HOMO level of the phenothiazine-based polymer is found to enhance the photovoltaic performance by increasing the open-circuit voltage of the polymer solar cell relative to the phenoxazine-based congener. At the same donor:acceptor blend ratio of 1:4, the light-harvesting capability and solar cell efficiency notably increase as the thienyl rings are added.

1. Introduction

The development of synthetic routes towards transition metal oligoynes and polyynes of the form *trans*-[−M(L)$_2$C≡C(R)C≡C−]$_n$ (L = auxiliary ligands, R = spacer unit) has shown much progress in the past few decades [1–5]. These main-chain organometallic oligomeric and polymeric functional materials are intriguing for their unique properties such as electrical conductivities, luminescence, nonlinear optical and photovoltaic properties, liquid crystallinity and chemosensing [1–5]. To date, a large library of soluble platinum(II) polyynes incorporating various conjugated carbocyclic and heteroaromatic ring systems have been prepared [3–5]. The advances in chemical synthesis have resulted in many application-oriented conjugated polymers of this kind that can give rise to diverse photophysics and materials properties. The generally good solubility of Pt-containing poly-(heteroarylene ethynylene)s over their organic analogues also favors good film formation. When Pt metal is conjugated with an alkyne unit, the Pt d-orbitals overlap with the p-orbitals of the alkyne unit, which leads to an enhancement of π-electron delocalization and intrachain charge transport along the main chain [3–5]. Efficient intersystem crossing in such organometallic species by enhancing the spin-orbit coupling in the presence of the heavy metal atom facilitates the formation of triplet excitons, which have longer lifetimes and thus allow extended exciton diffusion lengths.

Phenothiazine (PTZ) and phenoxazine (POZ) are both heteroanthracene derivatives and represent two important classes of tricyclic nitrogen–sulfur and nitrogen–oxygen heterocycles, respectively [6]. Organic dyes containing PTZ and POZ have recently attracted much research interest because of their excellent hole-transporting ability, rigid structure and large π-conjugated skeleton [6,7]. In many push-pull organic dyes incorporating PTZ and POZ, the nonplanar configuration could also impede the molecular aggregation and the formation of intermolecular excimers [8]. Furthermore, many studies have shown that alkylthio substitution in conjugated polymers has made a profound impact on improving

* Corresponding author.
** Corresponding author. Department of Applied Biology and Chemical Technology, The Hong Kong Polytechnic University, Hung Hom, Hong Kong, China.
E-mail addresses: wai-yeung.wong@polyu.edu.hk (W.-Y. Wong), wl@szu.edu.cn (L. Wang).

https://doi.org/10.1016/j.jorganchem.2019.06.035
0022-328X/

the photovoltaic performance of these donor materials in polymer solar cells (PSCs) [9,10]. Previously, the synthesis and properties of platinum(II) polyyne polymers with PTZ spacer have been described [11]. The POZ exhibits similar structural and redox properties to PTZ, indicating that POZ should be equally interesting to be incorporated into the dyes [12]. In fact, POZ dyes have also been utilized in other applications such as laser dyes [13], hole-transporting materials [14], indicators [15] and host-guest systems [16]. Like PTZ, an important feature of POZ is the ease of structural modification on both sides of the POZ core to tune the absorption and electronic properties of the organic chromophore in the dye. Here, we report the synthesis and characterization of new conjugated organometallic polymers with alternating thiophene-flanked POZ moieties and *trans*-Pt(PBu_3)$_2$ acetylide units (**P1**–**P2** in Chart 1) and their model compounds. Studies of the photophysical, thermal stability and electrochemical properties of these polyplatinynes were conducted. A comparison between POZ- and PTZ-based polymers was also made (Chart 1).

2. Materials and methods

2.1. Materials and instruments

All reactions were carried out under a nitrogen atmosphere by using standard Schlenk techniques. Solvents were dried and distilled from appropriate drying agents under an inert atmosphere prior to use. All reagents and chemicals, unless otherwise stated, were purchased from commercial sources and used without further purification. *trans*-Pt(PEt_3)$_2$(Ph)Cl [17] and *trans*-Pt(PBu_3)$_2$$Cl_2$ [18] were prepared according to the literature methods. All reactions were monitored by thin-layer chromatography (TLC) with Merck pre-coated glass plates. Flash column chromatography and preparative TLC were carried out using silica gel from Merck (230–400 mesh).

Infrared spectra were recorded as KBr pellets using a Perkin Elmer Paragon 1000 PC or Nicolet Magna 550 Series II FT-IR spectrometer, using CaF_2 cells with a 0.5 mm path length. Fast atom bombardment (FAB) mass spectra were recorded on a Finnigan MAT SSQ710 system and MALDI-TOF (matrix-assisted laser desorption/ionization time-of-flight) spectra were obtained by a Autoflex Bruker MALDI-TOF mass spectrometer. NMR spectra were measured in $CDCl_3$ on a Varian Inova 400 MHz FT-NMR spectrometer and chemical shifts were quoted relative to tetramethylsilane for ^{1}H and ^{13}C nuclei and H_3PO_4 for ^{31}P nucleus.

The cyclic voltammograms were acquired with a CHI model 600D electrochemical station in deoxygenated acetonitrile containing 0.1 M [Bu_4N]PF_6 as the supporting electrolyte. A conventional three-electrode configuration consisting of a platinum working electrode, a Pt-wire counter electrode and a Ag/AgCl reference electrode was used. The polymer films were casted on the ITO covered glass. All potentials reported were quoted with reference to the ferrocene-ferrocenium (Fc/Fc^+) couple at a scan rate of 100 mV s^{-1}.

2.2. Synthesis

2.2.1. Synthesis of 10-hexadecylphenoxazine

10*H*-Phenoxazine (500 mg, 2.73 mmol), 1-bromohexadecane (1.0 g, 3.27 mmol) and KOH (1.5 g, 27.3 mmol) were added to DMSO (10 mL), and the solution was stirred vigorously at room temperature for 24 h. Water was added, and the reaction mixture was extracted with ethyl acetate. The extract was washed with water and dried over anhydrous magnesium sulfate. After removing the solvent using a rotary evaporator, the crude product was purified by column chromatography on silica gel eluting with *n*-hexane to provide 10-hexadecylphenoxazine (996 mg, 90%) as a white solid. ^{1}H NMR (400 MHz, $CDCl_3$): δ = 6.79–6.75 (m, 2H, Ar), 6.64–6.59 (m, 4H, Ar), 6.44 (d, J = 7.7 Hz, 2H, Ar), 3.45 (t, J = 8.0 Hz, 2H, $NCH_2(CH_2)_{14}CH_3$), 1.66–1.61 (m, 2H, $NCH_2CH_2(CH_2)_{13}CH_3$), 1.37–1.26 (m, 26H, $NCH_2CH_2(CH_2)_{13}CH_3$), 0.88 (t, J = 6.5 Hz, 3H, $NCH_2CH_2(CH_2)_{13}CH_3$) ppm. ^{13}C NMR (100 MHz, $CDCl_3$): δ = 145.34, 133.76, 123.92, 120.96, 115.63, 111.57 (Ar), 44.43, 32.29, 30.06, 30.05, 30.03, 30.00, 29.99, 29.94, 29.76, 29.73, 27.28, 25.19, 23.05, 14.49 ($C_{16}H_{33}$) ppm. FAB-MS (*m/z*): 408 $[M+1]^+$.

2.2.2. Synthesis of 2,7-dibromo-10-hexadecylphenoxazine (**L1-2Br**)

10-Hexadecylphenoxazine (295 mg, 0.72 mmol) was dissolved in $CHCl_3$ (15 mL), and bromine (243 mg, 1.5 mmol) was added dropwise. The reaction mixture was stirred at room temperature in the dark overnight. Na_2SO_3 solution was added, and the reaction mixture was extracted with ethyl acetate. The extract was washed with water and dried over anhydrous magnesium sulfate. After removing the solvent using a rotary evaporator, the crude product was purified by column chromatography on silica gel eluting with hexane to provide 2,7-dibromo-10-hexadecylphenoxazine (373 mg, 91%) as a white solid. ^{1}H NMR (400 MHz, $CDCl_3$): δ = 6.86 (dd, J = 1.8 Hz, J = 8.5 Hz, 2H, Ar), 6.70 (d, J = 1.8 Hz, 2H, Ar), 6.26 (d, J = 8.5 Hz, 2H, Ar), 3.35 (t, J = 7.1 Hz, 2H, $NCH_2(CH_2)_{14}CH_3$), 1.57–1.56 (m, 2H, $NCH_2CH_2(CH_2)_{13}CH_3$), 1.35–1.26 (m, 26H, $NCH_2CH_2(CH_2)_{13}CH_3$), 0.88 (t, J = 6.6 Hz, 3H, $NCH_2CH_2(CH_2)_{13}CH_3$) ppm. ^{13}C NMR (100 MHz, $CDCl_3$): δ = 145.48, 132.46, 126.83, 118.85, 112.69, 112.47 (Ar), 44.56, 32.27, 30.05, 30.01, 29.97, 29.92, 29.90, 29.71, 29.68, 27.15, 24.97, 23.04, 14.48 ($C_{16}H_{33}$) ppm. FAB-MS (*m/z*): 565 $[M+1]^+$.

2.2.3. Synthesis of **L2-2Br**

To a solution of **L1-2Br** (248 mg, 0.44 mmol) in freshly distilled THF (30 mL) was added $Pd(PPh_3)_4$ (101 mg) and the mixture was stirred at room temperature for 30 min. Thiophen-2-yl-2-boronic acid (280 mg, 2.2 mmol) and Na_2CO_3 (2 M, aqueous, 1.8 mL) were added sequentially. The mixture was stirred at 80 °C for 24 h. The solvent was evaporated and water (30 mL) was added to the residue which was extracted into CH_2Cl_2 (3 × 20 mL). The organic layer was dried over $MgSO_4$, then concentrated under reduced pressure and purified by chromatography on an aluminium oxide column eluting with *n*-hexane/CH_2Cl_2 (5:1, v/v) to provide compound **L1-2Th** (195 mg, 71%) as a yellow solid. ^{1}H NMR (400 MHz, $CDCl_3$): δ = 7.20–7.16 (m, 4H, Ar), 7.07–7.03 (m, 4H, Ar), 6.91 (d, J = 2.1 Hz, 2H, Ar), 6.45 (d, J = 8.4 Hz, 2H, Ar), 3.49 (t, J = 7.9 Hz, 2H, $NCH_2(CH_2)_{14}CH_3$), 1.69–1.65 (m, 2H, $NCH_2CH_2(CH_2)_{13}CH_3$), 1.39–1.27 (m, 26H, $NCH_2CH_2(CH_2)_{13}CH_3$), 0.89 (t, J = 6.6 Hz, 3H, $NCH_2CH_2(CH_2)_{13}CH_3$) ppm. ^{13}C NMR (100 MHz, $CDCl_3$): δ = 145.06, 144.03, 132.51, 128.24, 127.80, 123.95, 122.13, 121.51, 113.21, 111.76 (Ar), 44.43, 32.28, 30.06, 30.02, 30.00, 29.96, 29.94, 29.74, 29.72, 27.25, 25.33, 23.05, 14.50 ($C_{16}H_{33}$) ppm. FAB-MS (*m/z*): 571 $[M+1]^+$.

Compound **L1-2Th** (180 mg, 0.29 mmol) was then dissolved in a mixture of chloroform (20 mL) and acetic acid (2 mL). *N*-Bromosuccimide (NBS, 107 mg, 0.60 mmol) was added to the solution and the mixture was stirred overnight in the dark. The solvents were removed on a rotary evaporator in *vacuo*. The crude product was purified by column chromatography on silica gel eluting with *n*-hexane/CH_2Cl_2 (5:1, v/v) to provide **L2-2Br** (188 mg, 90%) as a yellow solid. ^{1}H NMR (400 MHz, $CDCl_3$): δ = 6.96 (d, J = 3.8 Hz, 2H, Ar), 6.93 (dd, J = 2.1 Hz, J = 8.4 Hz, 2H, Ar), 6.87 (d, J = 3.8 Hz, 2H, Ar), 6.77 (d, J = 2.1 Hz, 2H, Ar), 6.42 (d, J = 8.4 Hz, 2H, Ar), 3.46 (t, J = 7.9 Hz, 2H, $NCH_2(CH_2)_{14}CH_3$), 1.64–1.62 (m, 2H, $NCH_2CH_2(CH_2)_{13}CH_3$), 1.37–1.26 (m, 26H, $NCH_2CH_2(CH_2)_{13}$ CH_3), 0.88 (t, J = 6.6 Hz, 3H, $NCH_2CH_2(CH_2)_{13}CH_3$) ppm. ^{13}C NMR (100 MHz, $CDCl_3$): δ = 145.41, 145.09, 132.76, 131.06, 127.09, 122.26, 121.35, 112.81, 111.87, 110.36 (Ar), 44.46, 32.28, 30.07, 30.03, 30.00,

29.95, 29.93, 29.72, 27.23, 25.32, 23.05, 14.49 ($C_{16}H_{33}$) ppm. FAB-MS (*m/z*): 729 $[M+1]^+$.

*2.2.4. Synthesis of **L1-2TMS***

To an ice-cooled mixture of **L1-2Br** (120 mg, 0.21 mmol) in freshly distilled triethylamine (10 mL) and CH_2Cl_2 (10 mL) solution under nitrogen was added $Pd(OAc)_2$ (16 mg), PPh_3 (50 mg) and CuI (5 mg). After the solution was stirred for 30 min, trimethylsilylacetylene (52 mg, 0.53 mmol) was then added and the suspension was stirred for another 30 min in the ice bath before being warmed to room temperature. After reacting for 30 min at room temperature, the mixture was heated to 50 °C for 24 h. The solution was then allowed to cool to room temperature and the solvents were removed on a rotary evaporator in *vacuo*. The crude product was purified by column chromatography on silica gel eluting with *n*-hexane/CH_2Cl_2 (5:1, v/v) to provide **L1-2TMS** (66 mg, 54%) as a yellow solid. IR (KBr): ν(C≡C) 2151 cm^{-1}. ^1H NMR (400 MHz, $CDCl_3$): δ = 6.91 (dd, *J* = 1.9 Hz, *J* = 8.4 Hz, 2H, Ar), 6.69 (d, *J* = 1.9 Hz, 2H, Ar), 6.34 (d, *J* = 8.4 Hz, 2H, Ar), 3.43 (t, *J* = 7.8 Hz, 2H, $NCH_2(CH_2)_{14}CH_3$), 1.61 (br, 2H, $NCH_2CH_2(CH_2)_{13}CH_3$), 1.37–1.28 (m, 26H, $NCH_2CH_2(CH_2)_{13}CH_3$), 0.91 (t, *J* = 6.6 Hz, 3H, $NCH_2CH_2(CH_2)_{13}CH_3$), 0.28 (s, 18H, $Si(CH_3)_3$) ppm. ^{13}C NMR (100 MHz, $CDCl_3$): δ = 144.42, 133.48, 128.45, 118.80, 115.66, 111.31 (Ar), 105.01, 93.29 (C≡C), 44.35, 32.28, 30.05, 30.04, 30.01, 29.98, 29.94, 29.91, 29.72, 29.69, 27.16, 25.24, 23.06, 14.50 ($C_{16}H_{33}$), 0.38 ($Si(CH_3)_3$) ppm. FAB-MS (*m/z*): 601 $[M+1]^+$.

*2.2.5. Synthesis of **L2-2TMS***

This compound was prepared in a similar way as **L1-2TMS**. A yellow solid. Eluent: hexane/CH_2Cl_2 (5:1, v/v). Yield: 69%. IR (KBr): ν(C≡C) 2142 cm^{-1}. ^1H NMR (400 MHz, $CDCl_3$): δ = 7.14 (d, *J* = 3.8 Hz, 2H, Ar), 6.98–6.95 (m, 4H, Ar), 6.80 (d, *J* = 2.1 Hz, 2H, Ar), 6.37 (d, *J* = 8.5 Hz, 2H, Ar), 3.40 (t, *J* = 7.6 Hz, 2H, $NCH_2(CH_2)_{14}CH_3$), 1.61 (br, 2H, $NCH_2CH_2(CH_2)_{13}CH_3$), 1.36–1.28 (m, 26H, $NCH_2CH_2(CH_2)_{13}CH_3$), 0.90 (t, *J* = 6.6 Hz, 3H, $NCH_2CH_2(CH_2)_{13}CH_3$), 0.28 (s, 18H, $Si(CH_3)_3$) ppm. ^{13}C NMR (100 MHz, $CDCl_3$): δ = 145.41, 144.94, 134.07, 132.71, 127.04, 121.76, 121.56, 121.20, 112.89, 111.76 (Ar), 99.61, 98.25 (C≡C), 44.37, 32.27, 30.06, 30.02, 29.96, 29.93, 29.72, 27.20, 25.30, 23.05, 14.50 ($C_{16}H_{33}$), 0.25 ($Si(CH_3)_3$) ppm. FAB-MS (*m/z*): 763 $[M+1]^+$.

*2.2.6. Synthesis of diethynyl ligand **L1***

A mixture of **L1-2TMS** (64 mg, 0.11 mmol) and K_2CO_3 (31 mg, 0.22 mmol) in methanol (6 mL) and CH_2Cl_2 (15 mL) solution mixture, under a nitrogen atmosphere, was stirred at room temperature overnight. The solvents were removed on a rotary evaporator in *vacuo*. The crude product was purified by column chromatography on silica gel eluting with *n*-hexane/CH_2Cl_2 (5:1, v/v) to provide **L1** (33 mg, 69%) as a yellow solid. IR (KBr): ν(C≡C) 2100, ν(C≡CH) 3276 cm^{-1}. ^1H NMR (400 MHz, $CDCl_3$): δ = 6.93 (dd, *J* = 1.9 Hz, *J* = 8.3 Hz, 2H, Ar), 6.70 (d, *J* = 1.9 Hz, 2H, Ar), 6.36 (d, *J* = 8.3 Hz, 2H, Ar), 3.43 (t, *J* = 8.0 Hz, 2H, $NCH_2(CH_2)_{14}CH_3$), 2.98 (s, 2H, C≡C*H*), 1.63–1.59 (m, 2H, $NCH_2CH_2(CH_2)_{13}CH_3$), 1.37–1.26 (m, 26H, $NCH_2CH_2(CH_2)_{13}CH_3$), 0.88 (t, *J* = 6.6 Hz, 3H, $NCH_2CH_2(CH_2)_{13}CH_3$) ppm. ^{13}C NMR (100 MHz, $CDCl_3$): δ = 144.51, 133.77, 128.69, 118.95, 114.65, 111.46 (Ar), 83.50, 76.55 (C≡C), 44.41, 32.27, 30.05, 30.01, 29.98, 29.93, 29.90, 29.72, 29.69, 27.17, 25.22, 23.05, 14.49 ($C_{16}H_{33}$) ppm. FAB-MS (*m/z*): 456 $[M+1]^+$.

*2.2.7. Synthesis of **L2***

This compound was prepared in a similar manner to **L1**. A yellow solid. Eluent: *n*-hexane/CH_2Cl_2 (5:1, v/v). Yield: 90%. IR (KBr): ν(C≡C) 2100, ν(C≡CH) 3305 cm^{-1}. ^1H NMR (400 MHz, $CDCl_3$): δ = 7.19 (d, *J* = 3.8 Hz, 2H, Ar), 7.01–6.98 (m, 4H, Ar), 6.83 (d, *J* = 2.1 Hz, 2H, Ar), 6.43 (d, *J* = 8.4 Hz, 2H, Ar), 3.46 (t, *J* = 7.6 Hz, 2H, $NCH_2(CH_2)_{14}CH_3$), 3.39 (s, 2H, C≡C*H*), 1.68–1.64 (m, 2H, $NCH_2CH_2(CH_2)_{13}CH_3$), 1.38–1.26 (m, 26H, $NCH_2CH_2(CH_2)_{13}CH_3$), 0.88 (t, *J* = 6.6 Hz, 3H, $NCH_2CH_2(CH_2)_{13}CH_3$) ppm. ^{13}C NMR (100 MHz, $CDCl_3$): δ = 145.75, 145.02, 134.50, 132.90, 127.01, 121.80, 121.72, 120.04, 113.05, 111.86 (Ar), 82.05, 77.62 (C≡C), 44.43, 32.27, 30.06, 30.02, 29.99, 29.95, 29.92, 29.72, 27.21, 25.31, 23.05, 14.50 ($C_{16}H_{33}$) ppm. FAB-MS (*m/z*): 620 $[M+1]^+$.

*2.2.8. Synthesis of platinum metallopolyyne **P1***

To a stirred mixture of **L1** (28 mg, 0.06 mmol) and *trans*-$[Pt(PBu_3)_2Cl_2]$ (41 mg 0.06 mmol) in freshly distilled triethylamine (8 mL) and CH_2Cl_2 (15 mL) solution was added CuI (3 mg). The solution was stirred at room temperature for 24 h under a nitrogen atmosphere. The solvents were removed on a rotary evaporator in *vacuo*. The residue was redissolved in CH_2Cl_2 and filtered through a short aluminium oxide column using the same eluent to remove ionic impurities and catalyst residue. After removal of the solvent, the crude product was washed with *n*-hexane three times followed by methanol three times and drying in *vacuo* to obtain **P1** (60 mg, 87%) as a yellow solid. IR (KBr): ν(C≡C) 2099 cm^{-1}.^1H NMR (400 MHz, $CDCl_3$): δ = 6.70 (d, *J* = 8.2 Hz, 2H, Ar), 6.68 (s, 2H, Ar), 6.27 (d, *J* = 8.2 Hz, 2H, Ar), 3.41 (br, 2H, alkyl), 2.11–2.08 (m, 12H, alkyl), 1.59–1.26 (m, 52H, alkyl), 0.95–0.86 (m, 21H, alkyl) ppm. ^{31}P NMR (161 MHz, $CDCl_3$): δ = 2.80 ($^1J_{P-Pt}$ = 2366 Hz) ppm.

*2.2.9. Synthesis of platinum metallopolyyne **P2***

Polymer **P2** was prepared in a similar manner to **P1** except that **L2** was used for the polycondensation. An orange solid. Yield: 32%. IR (KBr): ν(C≡C) 2089 cm^{-1}.^1H NMR (400 MHz, $CDCl_3$): δ = 6.99–6.42 (m, 10H, Ar), 3.49 (br, 2H, alkyl), 2.11–2.10 (m, 12H, alkyl), 1.60–1.26 (m, 52H, alkyl), 0.97–0.86 (m, 21H, alkyl) ppm. ^{31}P NMR (161 MHz, $CDCl_3$): δ = 3.24 ($^1J_{P-Pt}$ = 2329 Hz) ppm.

*2.2.10. Synthesis of platinum model complex **M1***

To a stirred mixture of ligand **L1** (10 mg, 0.022 mmol) and *trans*-$[PtPh(Cl)(PEt_3)_2]$ (24 mg, 0.044 mmol) in NEt_3 (6 mL) and CH_2Cl_2 (8 mL), CuI (2 mg) was added as the catalyst. The solution was stirred at room temperature overnight under nitrogen, after which all volatile components were removed under vacuum. The crude product was taken up in CH_2Cl_2 and purified on preparative silica TLC plates with *n*-hexane/EtOAc (5:1, v/v) as eluent to provide **M1** (18 mg, 56%) as a light-yellow solid. IR (KBr): ν(C≡C) 2095 cm^{-1}. ^1H NMR (400 MHz, $CDCl_3$): δ = 7.36–7.29 (m, 4H, Ar), 6.97–6.93 (m, 4H, Ar), 6.81–6.73 (m, 4H, Ar), 6.57 (br, 2H, Ar), 6.29 (d, *J* = 8.1 Hz, 2H, Ar), 3.42 (t, *J* = 6.7 Hz, 2H, $NCH_2(CH_2)_{14}CH_3$), 1.77–1.70 (m, 26H, PCH_2CH_3 + $NCH_2CH_2(CH_2)_{13}CH_3$), 1.35–1.26 (m, 26H, $NCH_2CH_2(CH_2)_{13}CH_3$), 1.20–1.04 (m, 36H, PCH_2CH_3), 0.88 (t, *J* = 6.6 Hz, 3H, $NCH_2CH_2(CH_2)_{13}CH_3$) ppm. ^{13}C NMR (100 MHz, $CDCl_3$): δ = 144.38, 139.55, 130.78, 127.56, 126.43, 121.84, 121.43, 117.90, 110.98 (Ar), 109.61 (C≡C), 44.36, 32.27, 30.04, 30.02, 30.00, 29.95, 29.79, 29.71, 27.30, 25.36, 23.04, 15.35, 14.48, 8.36 (PEt_3 + $C_{16}H_{33}$) ppm. ^{31}P NMR (161 MHz, $CDCl_3$): δ = 9.73 ($^1J_{P-Pt}$ = 2641 Hz) ppm. FAB-MS (*m/z*): 1470 $[M+1]^+$.

*2.2.11. Synthesis of platinum model complex **M2***

Complex **M2** was made in a similar manner to **M1** except that **L2** was used instead of **L1**. A yellow solid. Eluent: *n*-hexane/EtOAc (5:1, v/v). Yield: 74%. IR (KBr): ν(C≡C) 2085 cm^{-1}.^1H NMR (400 MHz, $CDCl_3$): δ = 7.35–7.28 (m, 4H, Ar), 7.00–6.93 (m, 8H, Ar), 6.85–6.77 (m, 6H, Ar), 6.42 (d, *J* = 8.5 Hz, 2H, Ar), 3.48 (t, *J* = 7.3 Hz, 2H, $NCH_2(CH_2)_{14}CH_3$), 1.78–1.64 (m, 26H, PCH_2CH_3 + $NCH_2CH_2(CH_2)_{13}CH_3$), 1.38–1.24 (m, 26H, $NCH_2CH_2(CH_2)_{13}CH_3$), 1.14–1.06 (m, 36H, PCH_2CH_3), 0.88 (t, *J* = 6.6 Hz, 3H, $NCH_2CH_2(CH_2)_{13}CH_3$) ppm. ^{13}C NMR (100 MHz, $CDCl_3$): δ = 145.01, 140.01, 139.41, 132.01, 128.95, 128.22, 128.15,

127.65, 121.63, 120.87, 112.68, 111.65 (Ar), 102.77 (C≡C), 44.40, 32.26, 30.04, 30.01, 29.98, 29.96, 29.93, 29.74, 29.71, 27.26, 25.37, 23.04, 21.40, 15.42, 14.48, 8.38 (PEt_3 + $C_{16}H_{33}$) ppm. ^{31}P NMR (161 MHz, $CDCl_3$): δ = 9.94 ($^1J_{P-Pt}$ = 2627 Hz) ppm. FAB-MS (*m/z*): 1634 $[M+1]^+$.

3. Results and discussion

3.1. Synthesis and characterization

Scheme 1 outlines the synthesis of ligand precursors **L1** and **L2**. First, 10*H*-phenoxazine was alkylated at the *N*-position using 1-bromohexadecane in the presence of potassium hydroxide in DMSO. Then, the *N*-alkylated product was brominated with 2 molar equivalents of bromine to afford **L1-2Br**. Compound **L1-2Br** was coupled with 2-thienylboronic acid to give compound **L1-2Th**. Then, **L2-2Br** was synthesized by the bromination of compound **L1-2Th** with NBS. The ligand precursors **L1-2Br** and **L2-2Br** reacted with trimethylsilylacetylene using copper iodide, palladium acetate and triphenylphosphine as the catalysts to give the **L1-2TMS** and **L2-2TMS**, respectively [5]. Then, the target diethynyl ligands were prepared by deprotecting the two TMS groups in the presence of potassium carbonate, using a mixture of dichloromethane and methanol as the solvent.

Scheme 2 depicts the synthesis of the platinum(II) metallopolyynes **P1**–**P2**. Both polymers were prepared by the dehydrohalogenation reaction between the corresponding ligands and platinum dichloride complex using copper iodide as the catalyst in a solution mixture of dichloromethane and trimethylamine [19]. They were purified by flash column chromatography over neutral Al_2O_3 to remove ionic impurities and catalyst residue, and repeated precipitation and isolation. In the same way that the polymers were synthesized, the dimers **M1**–**M2** can also be prepared by the dehydrohalogenation reaction between the corresponding ligands and platinum chloride complex (Scheme 2) [20]. These dinuclear complexes can be used as good molecular model systems to investigate the spectroscopic and photophysical properties of the polymers.

All the ligands, polymers and newly synthesized compounds are air-stable solids and can be stored without any special precautions. They were well characterized by common spectroscopic techniques including NMR spectroscopy, infrared spectroscopy and FAB mass spectrometry. ^1H NMR analysis clearly demonstrates a well-defined structure for each of the compounds. In all cases, ^1H resonances stemming from the protons of the organic moieties were observed. All the proton signals of aryl rings are on the downfield side and the terminal acetylenic proton (C≡C–H) signals are located at around 3.5 ppm as a sharp signal, while the alkyl proton signals appear on the high-field side. The ^{13}C NMR spectral data give precise information about the regiochemical structure of all the compounds synthesized. There are distinct signals (i.e. 80–110 ppm) for the individual sp carbons. All the aromatic carbons were clearly identified in the aromatic region (i.e. 120–170 ppm), and all the sp^3 carbons were observed in the alkyl region (i.e. < 60 ppm). The single ^{13}P NMR signals flanked by platinum satellites for the platinum complexes are consistent with a *trans* geometry of the square-planar Pt unit. The $^1J_{P-Pt}$ values of 2329–2366 Hz for the PBu_3 groups and 2627–2641 Hz for the PEt_3 ligands are typical of those

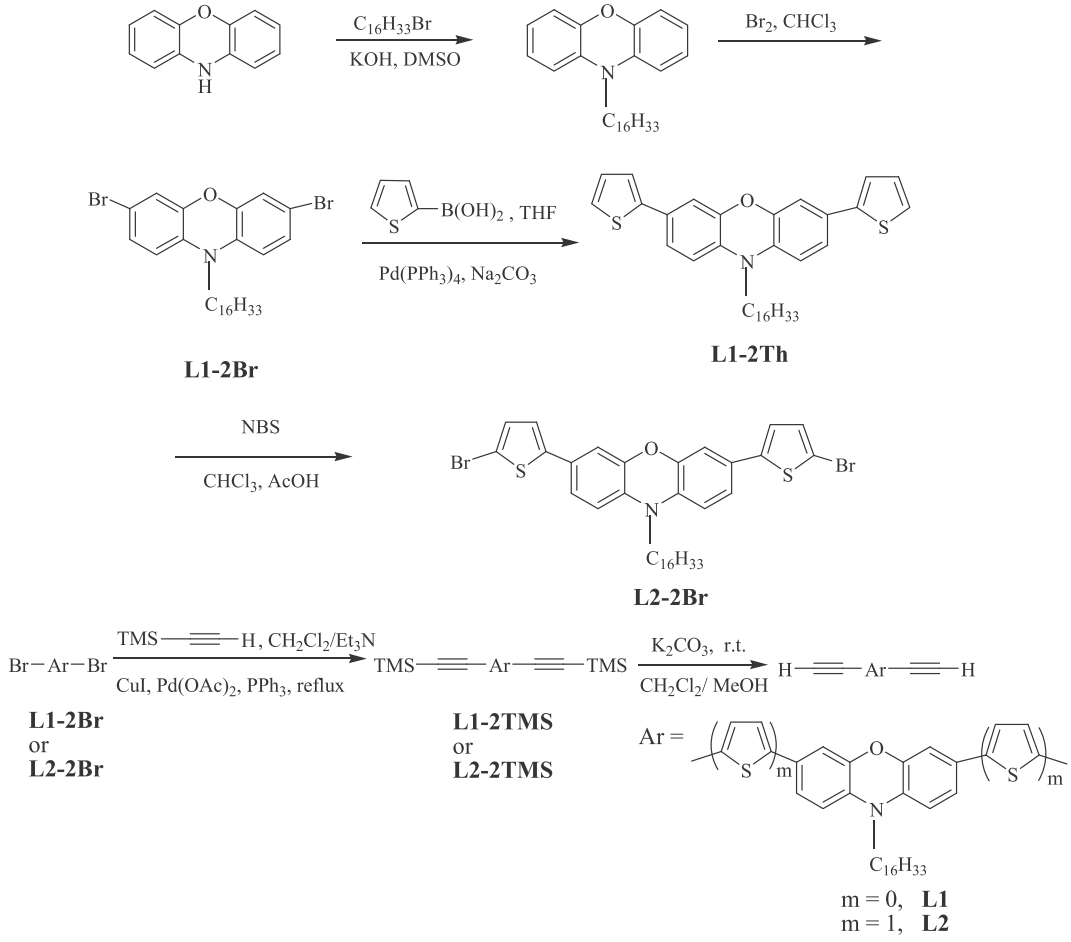

Scheme 1. Synthesis of ligand precursors **L1** and **L2**.

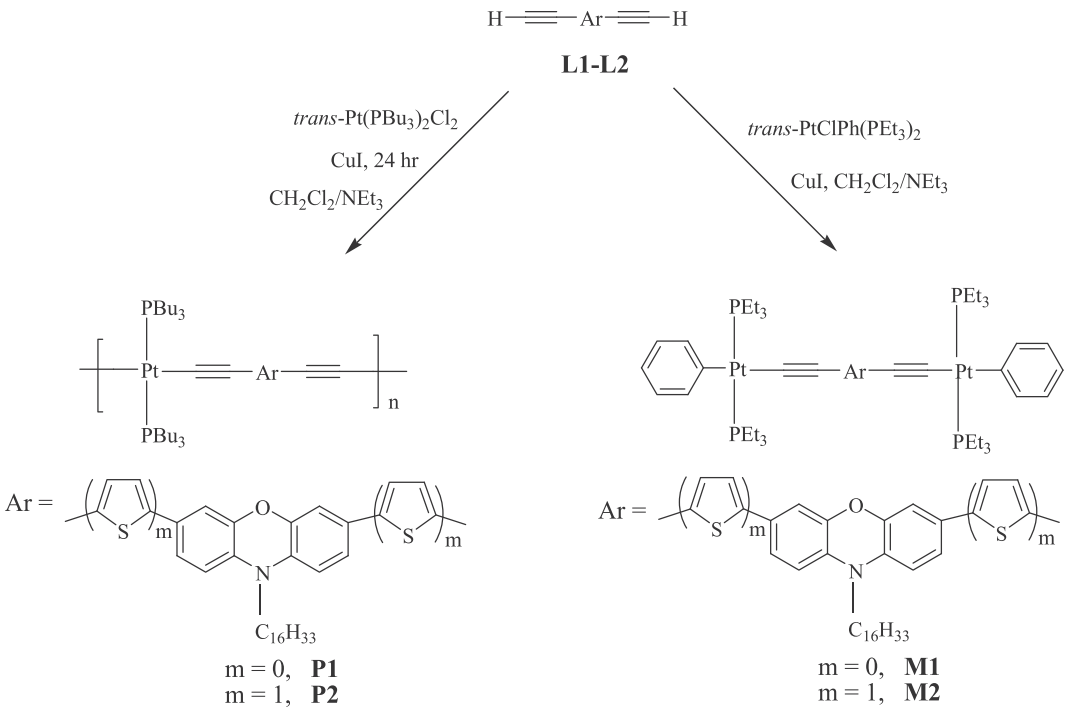

Scheme 2. Synthesis of Pt(II) metallopolyynes **P1**–**P2** and their model complexes **M1**–**M2**.

for related *trans*-PtP_2 systems, which are notably smaller than those of the corresponding *cis*-isomers (>3500 Hz) [21].

All the ligands, ligand precursors, polymers and model complexes which contain –C≡C- are subjected to IR measurements. All of them display IR ν(C≡C) absorptions near 2090 cm^{-1}. The terminal C≡C–H stretching vibrations occur at about 3300 cm^{-1}. The IR spectra of all Pt polymers and model complexes show no band characteristic of C≡C–H stretching vibration in the range of 3200–3300 cm^{-1} and this indicates that all the ligands are capped by metal groups via M – C σ bonds. The molecular formulae of all molecular compounds were successfully established by appearance of the intense molecular ion peaks in their positive FAB mass spectra.

3.2. Optical absorption and photoluminescence spectroscopies

The photophysical properties of all the ligands and metal-containing complexes have been characterized by UV–vis and photoluminescence (PL) spectroscopies. The absorption and emission spectra of the ligands, polymers and model complexes were measured in CH_2Cl_2 solutions. Relevant data are collected in Tables 1 and 2.

Figs. 1 and 2 show the absorption spectra of the POZ-based Pt compounds, and the data are also compared with those for the ligands (λ_{max} = 263, 382 nm for **L1** and 302, 427 nm for **L2**). Both polymers show broad absorption bands in the UV and visible region, which are ascribed to ligand-centered π-π* transitions [11]. The absorption wavelengths of the polymers are longer than those of the corresponding ligands. That is to say, the absorption bands of ligands are red-shifted when the platinum group is introduced, *i.e.*, on going from **L1** (or **L2**) to **P1** (or **P2**), and this reveals that π-conjugation of the ligands extends through the metal center. In comparison with **P1**, the addition of two thienyl rings on each side of POZ in **P2** shifts the absorption bands towards the longer wavelength (from 412 to 427 nm), which is ascribed to a higher degree of conjugation with the additional thienyl units. Besides, the absorption patterns of the diplatinum model compounds **M1** and **M2** are very similar to those of their polymeric congeners **P1** and **P2**. It is worth noting that the main absorption bands of **P1** and **P2** (412 and 427 nm, respectively) are more red-shifted than those of the corresponding S derivatives (349 and 412 nm for **P1**–**S** and **P2**–**S**, respectively) [11], which can be attributed to the stronger electron-donating ability of the O atom than that of the S atom in the heteroanthracene ring [9,10].

Figs. 3 and 4 show the emission spectra of the POZ-based ligands, polymers and model complexes. All these compounds emit strong fluorescence from the singlet excited states at 415–486 nm under ambient conditions. The measured PL lifetimes for **L1**–**L2**, **P1**–**P2** and **M1**–**M2** for the main peaks are all very short (ca. 0.65–4.85 ns) at 293 K, characteristic of the spin-allowed singlet emission. These results together with the small Stokes shift observed preclude the emitting state as a triplet excited state [22]. While a strong triplet emission at 544 (532) nm, with a substantially larger Stokes shift and a long triplet emissive lifetime τ_p of ca. 257.1 (61.4) μs, is detectable in the PL spectrum of **P1** (**M1**) at 77 K, we observed no such long-lived emission over the measured spectral window for **P2** (**M2**). The observation of efficient triplet emission is intrinsically more difficult for low-bandgap polyyne **P2**, which manifests the fate of energy gap law for Pt-containing conjugated polyynes and their model diynes [23]. Theoretically, the law predicts that the rate of radiationless deactivation increases as the emission gap decreases due to the matching of wavefunctions

Table 1
Absorption and emission data of ligands **L1**–**L2**.

Ligand	λ_{abs} (nm)[a]	λ_{em} (nm)[b]	Φ (%)[c]	E_g (eV)[d]
L1	263 (13.0), 382 (3.6)	415 (5.33)	80.54	2.97
L2	302 (5.9), 427 (5.2)	459 (2.53)	48.15	2.61

[a] In CH_2Cl_2 at 293 K. Extinction coefficients (10^4 M^{-1} cm^{-1}) are shown in parentheses.
[b] Lifetimes (ns) shown in parentheses were measured in CH_2Cl_2 solutions at 293 K.
[c] Quantum yield (%) shown in parentheses were measured in CH_2Cl_2 solutions at 293 K.
[d] Optical bandgaps were determined from onset of absorption in solutions.

Table 2
Absorption and emission data of Pt polymers **P1**–**P2** and **M1**–**M2**.

Polymer	λ_{abs} (nm)[a]	λ_{em} (nm)[b]		Φ (%)[d]	E_g (eV)[e]
		293 K	77 K		
P1	230, 268, 412	442 (4.85)	544 (257.1)[c]	2.17	2.82
P2	230, 367, 427	486 (0.80)	494 (0.95)	0.90	2.59
M1	230 (5.9), 271 (6.8), 389 (3.1)	424 (0.65)	532 (61.4)[c]	7.97	2.92
M2	230 (6.5), 260 (3.0), 431 (4.4)	480 (1.40)	483 (1.15)	3.73	2.61

[a] In CH_2Cl_2 at 293 K. Extinction coefficients ($10^4\ M^{-1}cm^{-1}$) are shown in parentheses.
[b] Lifetimes (ns) shown in parentheses were measured in CH_2Cl_2 solutions.
[c] Lifetimes (μs) shown in parentheses were measured in CH_2Cl_2 solutions.
[d] Quantum yield (%) shown in parentheses were measured in CH_2Cl_2 solutions at 293 K.
[e] Optical bandgaps were determined from onset of absorption in solutions.

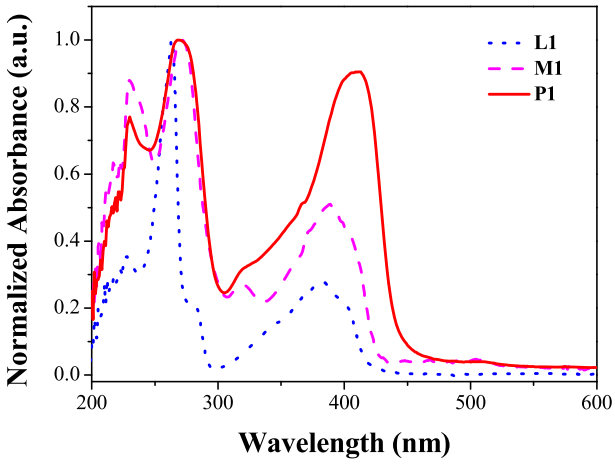

Fig. 1. Absorption spectra of **L1**, **M1** and **P1** at 293 K.

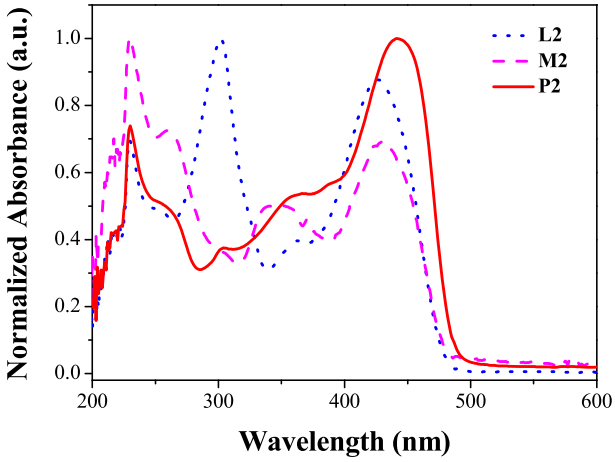

Fig. 2. Absorption spectra of **L2**, **M2** and **P2** at 293 K.

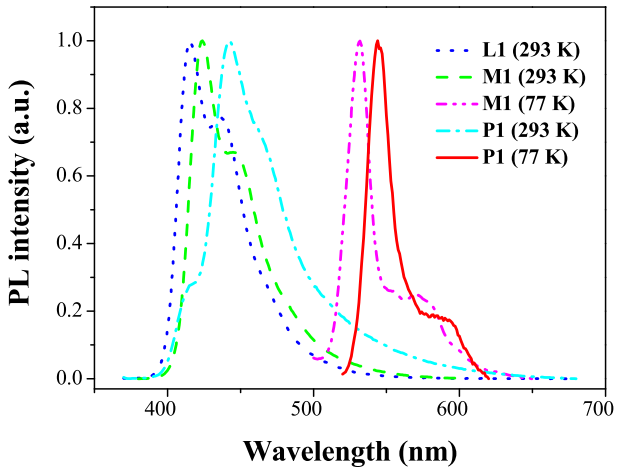

Fig. 3. Emission spectra of **L1**, **M1** and **P1**.

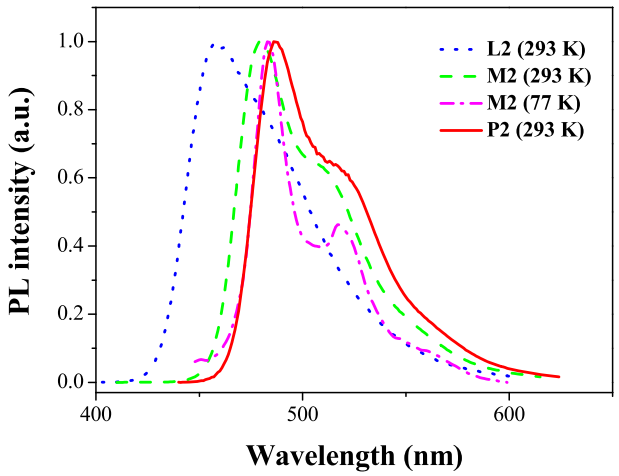

Fig. 4. Emission spectra of **L2**, **M2** and **P2**.

between the emitting state and highly vibrational levels of the ground electronic state, resulting in a fast $T_1 \rightarrow S_0$ internal conversion, followed by the solvent (or lattice in the solid state) deactivation [24]. This quenching mechanism is intrinsic and probably poses the main obstacle for phosphorescence for **P2** and **M2**. In addition, the fully extended heteroaryl rings in the ligand chromophore greatly reduce the effect of heavy metal ion in **P2** and **M2** which is mainly responsible for the intersystem crossing and hence the phosphorescence emission [25–27]. Similar to the absorption features, the fluorescence bands of **M2** and **P2** show bathochromic shifts in wavelength with respect to those of **M1** and **P1**, respectively, owing to the more conjugated backbone in the presence of two more thiophene rings. Such red-shift is also valid for the phosphorescence peak wavelength at 77 K by comparing the dimer **M1** and polymer **P1**.

3.3. Thermal gravimetric analysis and molecular weight determination of polymers

The molecular weights of the polymers were determined by Gel-Permeation Chromatography (GPC) in THF solution (Table 3).

Table 3
GPC and TGA results of polymers **P1**–**P2**.

Polymer	M_n[a]	M_w[b]	PDI[c]	DP[d]	T_{dec} (°C)[e]
P1	10090	19730	1.96	10	392
P2	29415	63740	2.17	24	374

[a] M_n = Number-average molecular weight.
[b] M_w = Weight-average molecular weight.
[c] PDI = Polydispersity Index.
[d] DP = Degree of polymerization based on M_n.
[e] Onset decomposition temperature.

These results indicate a moderate to high degree of polymerization and these data suggest a macromolecular nature of the materials. Polydispersity index (PDI) close to 2 has also been calculated in each case, which is a common value for polycondensates.

The thermal properties of the polymers were also examined by Thermal Gravimetric Analysis (TGA) under nitrogen (Table 3). Analysis of the TGA trace (heating rate 5 °C/min) for the polymers shows that they have onset decomposition temperatures $T_{dec} > 370$ °C, indicating that all the polymers exhibit very good thermal stability.

3.4. Redox properties and electronic energy levels of polymers

The highest occupied molecular orbital (HOMO) and the lowest unoccupied molecular orbital (LUMO) levels of stable polymers **P1**–**P2** were calculated based on the redox potentials determined from electrochemical measurements using cyclic voltammetry. The experiments were performed by casting the polymer films on the ITO covered glass working electrode with a Ag/AgCl wire as the reference electrode, at a scan rate of 100 mV s^{-1}. The solvent in all measurements was deoxygenated MeCN, and the supporting electrolyte was 0.1 M $[^nBu_4N]PF_6$. The relevant data are collected in Table 4. From the onset values of oxidation potential ($E_{onset,\ ox}$) and reduction potential ($E_{onset,\ red}$), the HOMO and LUMO levels of the polymers were calculated according to the following equations $E_{HOMO} = -(E_{onset,\ ox} + 4.72)$ eV and $E_{LUMO} = -(E_{onset,\ red} + 4.72)$ eV (where the unit of potential is V versus Ag/AgCl) [28]. For **P1** and **P2**, the oxidation potential (E_{ox}) was used to determine the HOMO energy level while the LUMO energy level was calculated based on the optical bandgap and the HOMO energy level determined. **P1** shows an oxidation potential at 0.80 eV (with the HOMO energy level of −5.52 eV and −2.70 eV for the LUMO energy level), while **P2** shows an oxidation potential at 0.73 eV (with the HOMO energy level of −5.45 eV and −2.86 eV for the LUMO energy level). This reveals that introduction of thiophene rings can elevate the HOMO level in **P2** relative to **P1**. As shown in Fig. 5, the red-shifted absorption and the down-shifted HOMO energy level of PTZ-derived polymer **P2**–**S** [11] make it a better donor material in PSCs as compared to that for the POZ-based counterpart **P2**.

Table 4
Electrochemical data and frontier orbital energy levels for **P1**–**P2**.

Polymer	E_{ox} (V)[a]	E_{red} (V)[a]	E_{HOMO} (eV)[b]	E_{LUMO} (eV)[b]	E_g^{ec} (eV)[c]	E_g^{opt} (eV)[d]
P1	+0.80	e	−5.52	−2.70[f]	e	2.82
P2	+0.73	e	−5[f]45	−2.86[f]	e	2.59

[e] Not observed.
[a] E_{ox} and E_{red} are the oxidation and reduction potentials, respectively.
[b] $E_{HOMO} = -(E_{ox} + 4.72$ eV and $E_{LUMO} = -(E_{red} + 4.72)$ eV.
[c] E_g^{ec} = Electrochemic[c]l bandgap.
[d] E_g^{opt} = Optical bandgap.
[f] Determined from $-(E_g^{opt} - E_{HUMO})$.

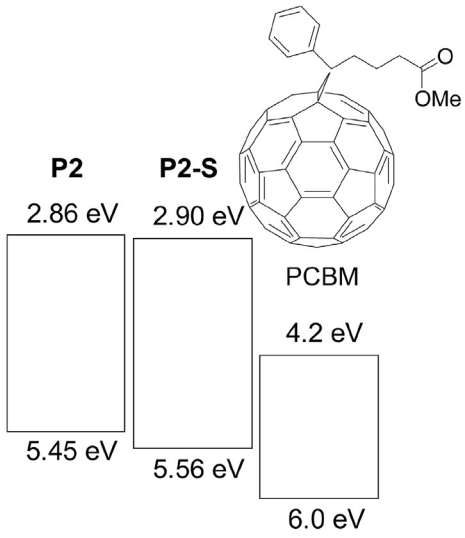

Fig. 5. Electronic energy levels of various PSC materials.

Table 5
Solar cell performance of devices fabricated with **P1**–**P2**.

Polymer	Spinning speed (rpm)	V_{oc} (V)	J_{sc} (mA cm^{-2})	FF	Efficiency (%)
P1	1000	0.52	1.00	0.45	0.23
P2	1000	0.43	2.40	0.36	0.37

3.4.1. Photovoltaic behavior of metallopolyyne polymers

Polymer solar cells (PSC) were fabricated by using the metallopolymers **P1** and **P2** developed in this section as an electron donor and PCBM as an electron acceptor. Relevant data are summarized in Table 5. The device structure was ITO/poly (3,4-ethylene-dioxythiophene):poly(styrene sulfonate) (PEDOT:PSS)/polymer:PCBM blend/Al. Indium tin oxide (ITO) glass substrates (10 Ω per square) were cleaned by sonication in toluene, acetone, ethanol, and deionized water, dried in an oven, and then cleaned with UV ozone for 300 s. As-received PEDOT:PSS solution was passed through the 0.45 μm filter and spin-coated on patterned ITO substrates at 5000 rpm for 3 min, followed by baking in N_2 at 150 °C for 15 min. The metallopolyyne:PCBM (1:4 by weight, unless

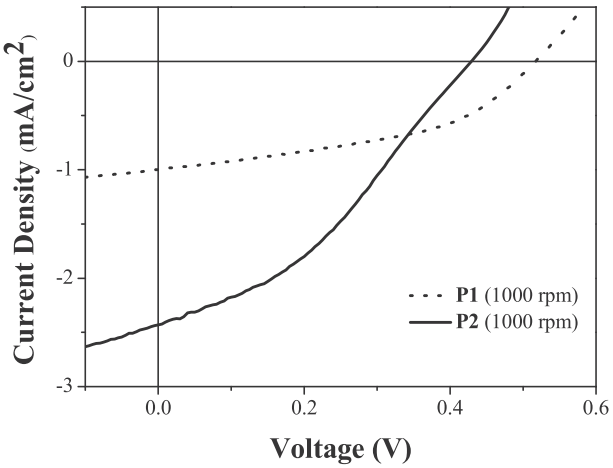

Fig. 6. *J-V* curves of solar cells with **P1**–**P2**:PCBM active layers under simulated AM 1.5 solar irradiation.

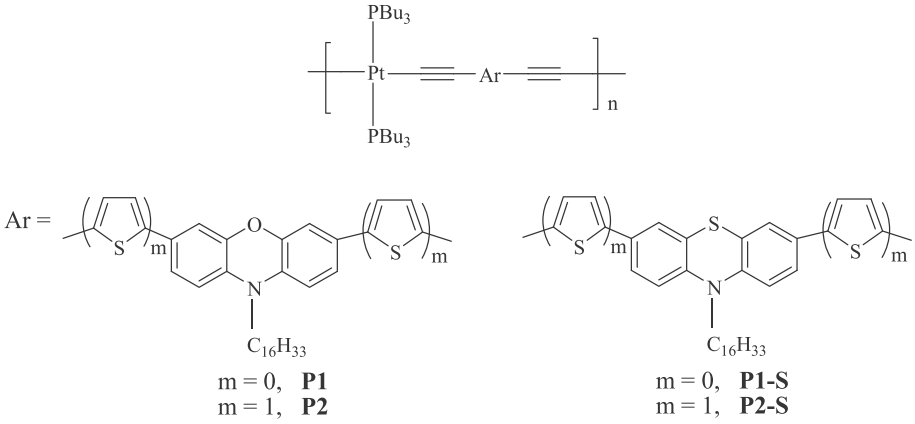

Chart 1. Comparison of polyplatinynes incorporating the phenoxazine and phenothiazine spacers.

specified otherwise) active layer was prepared by spin-coating the chlorobenzene solution (4 mg/mL of metallopolyyne, 16 mg/mL of PCBM) at 1000 rpm for 2 min. The substrates were dried at room temperature under low vacuum (vacuum oven) for 1 h and then stored under high vacuum (10^{-5}–10^{-6} Torr) overnight. An Al electrode (100 nm) was evaporated through a shadow mask to define the active area of the devices (2 mm^2 circle). All the fabrication procedures (except drying, PEDOT:PSS annealing, and Al deposition) and cell characterization were performed in air. Power conversion efficiency was determined from *J-V* curve measurement (using a Keithley 2400 sourcemeter) under white light illumination (at 100 mW/cm^2). For white light efficiency measurements, an Oriel 66002 solar light simulator with an AM 1.5 filter was used. The light intensity was measured by a Molectron Power Max 500D laser power meter.

Fig. 6 portrays the current density-voltage (*J-V*) characteristics of the PSCs recorded under AM 1.5 simulated solar illumination. It can be clearly observed that enhancing the absorption coefficient of the band by increasing the conjugation length of the chain with thienyl rings is a good strategy. A considerable increase in the short-circuit current density (J_{sc}) and power conversion efficiency (PCE) can be observed in **P2** (J_{sc} = 2.40 mA cm^{-2}, PCE = 0.37%) as compared with the corresponding polymer without thienyl rings **P1** (J_{sc} = 1.00 mA cm^{-2}, PCE = 0.23%). As expected from the above data on the HOMO levels, it is consistent with the result that **P2**–**S** gave a higher V_{oc} (0.63 V) and PCE (0.55%) than **P2** (Table 5) [11].

4. Conclusion

In summary, new polyplatinynes based on the phenoxazine-oligothiophene unit were designed and synthesized for comparing the optical, electronic and photovoltaic performance with the phenothiazine analogues. It is found that the sulfur derivative down-shifted the HOMO energy level by ca. 0.11 eV and slightly blue-shifted the absorption profile of the conjugated polymer as compared to the corresponding oxygen counterpart. This is in line with the effect of substitution of electron-donating atom. Due to the down-shifted HOMO level of **P2**–**S** relative to **P2**, the PSC device based on **P2**–**S** showed an enhanced V_{oc} of 0.63 V relative to that of 0.43 V for **P2**, causing a better PCE for the phenothiazine-based polymer. The results corroborate with the notion that molecular control by using sulfur atom instead of oxygen unit will hold great promise in broadening the absorption, down-shifting the HOMO level and hence improving the photovoltaic behavior of PSCs.

Acknowledgements

W.-Y.W. thanks the Hong Kong Research Grants Council (PolyU 123384/16P) and the Hong Kong Polytechnic University (1-ZE1C and 847S) for the financial support. We also acknowledge the assistance from Dr. Kai-Yin Cheung on the photovoltaic fabrication and testing.

References

[1] G.R. Whittell, M.D. Hager, U.S. Schubert, I. Manners, Nat. Mater. 10 (2011) 176–188.
[2] K.A. Williams, A.J. Boydstona, C.W. Bielawski, Chem. Soc. Rev. 36 (2007) 729–744.
[3] C.-L. Ho, W.-Y. Wong, Coord. Chem. Rev. 257 (2013) 1614–1649.
[4] C.-L. Ho, Z.-Q. Yu, W.-Y. Wong, Chem. Soc. Rev. 45 (2016) 5264–5295.
[5] A. Haque, R.A. Al-Balushi, I.J. Al-Busaidi, M.S. Khan, P.R. Raithby, Chem. Rev. 118 (2018) 8474–8597.
[6] M. Liang, J. Chen, Chem. Soc. Rev. 42 (2013) 3453–3488.
[7] K.M. Karlsson, X. Jiang, S.K. Eriksson, E. Gabrielsson, H. Rensmo, A. Hagfeldt, L. Sun, Chem. Eur J. 17 (2011) 6415–6424.
[8] H. Tian, X. Yang, J.Y. Cong, R. Chen, J. Liu, Y. Hao, A. Hagfeldt, L. Sun, Chem. Commun. (2009) 6288–6290.
[9] C. Cui, W.-Y. Wong, Y. Li, Energy Environ. Sci. 7 (2014) 2276–2284.
[10] C. Cui, W.-Y. Wong, Macromol. Rapid Commun. 37 (2016) 287–302.
[11] W.-Y. Wong, W.-C. Chow, K.-Y. Cheung, M.-K. Fung, A.B. Djurišić, W.-K. Chan, J. Organomet. Chem. 694 (2009) 2717–2726.
[12] X.Q. Zhu, Z. Dai, A. Yu, S.A. Wu, J.P. Cheng, J. Phys. Chem. B 112 (2008) 11694–11707.
[13] T.G. Pavlopoulos, Appl. Opt. 36 (1997) 4969–4980.
[14] R. Paspirgelyte, J.V. Grazulevicius, S. Grigalevicius, V. Jankauskas, Synth. Met. 159 (2009) 1014–1018.
[15] V.H.J. Frade, P.J.G. Coutinho, J.C.V.P. Moura, M.S.T. Goncalves, Tetrahedron 63 (2007) 1654–1663.
[16] H. Maas, A. Khatyr, G. Calzaferri, Microporous Mesoporous Mater. 65 (2003) 233–242.
[17] J. Chatt, B.L. Shaw, J. Chem. Soc. (1959) 4020–4033.
[18] J. Chatt, R.G. Hayter, J. Chem. Soc., Dalton Trans. (1961) 896–904.
[19] S. Takashahi, M. Kariya, T. Yatake, K. Sonogashira, N. Hagihara, Macromolecules 11 (1978) 1063–1066.
[20] J. Lewis, N.J. Long, P.R. Raithby, G.P. Shields, W.-Y. Wong, M. Younus, J. Chem. Soc., Dalton Trans. (1997) 4283–4288.
[21] S.O. Grim, R.L. Keiter, W. McFarlane, Inorg. Chem. 6 (1967) 1133–1137.
[22] F. Guo, Y.G. Kim, J.R. Reynolds, K.S. Schanze, Chem. Commun. (2006) 1887–1889.
[23] J.S. Wilson, N. Chawdhury, M.R.A. Al-Mandhary, M. Younus, M.S. Khan, P.R. Raithby, A. Köhler, R.H. Friend, J. Am. Chem. Soc. 123 (2001) 9412–9417.
[24] S.D. Cummings, R. Eisenberg, J. Am. Chem. Soc. 118 (1996) 1949–1960.
[25] N. Chawdhury, A. Kohler, R.H. Friend, W.-Y. Wong, J. Lewis, M. Younus, P.R. Raithby, T.C. Corcoran, M.R.A. Al-Mandhary, M.S. Khan, J. Chem. Phys. 110 (1999) 4963–4970.
[26] M. An, X. Yan, Z. Tian, J. Zhao, B. Liu, F. Dang, X. Yang, Y. Wu, G. Zhou, Y. Ren, L. Gao, J. Mater. Chem. C 4 (2016) 5626–5633.
[27] Z. Huang, B. Liu, Y. He, X. Yan, X. Yang, X. Xu, G. Zhou, Y. Ren, Z. Wu, J. Organomet. Chem. 794 (2015) 1–10.
[28] J. Hou, Z. Tan, Y. Yan, Y. He, C. Yang, Y. Li, J. Am. Chem. Soc. 128 (2006) 4911–4916.